Study on Surface Enhanced Raman Scattering of Au and Au@Al_2O_3 Spherical Dimers Based on 3D Finite Element Method

Baoxin Yan
Yanshan University
Yanying Zhu
Yanshan University
Yong Wei (wp921@ysu.edu.cn)
Yanshan University
Huan Pei
Yanshan University

Research Article

Keywords: Surface enhanced Raman scattering, Local plasmon, Gold nanospheres, Core-shell nanoparticles, Finite element method

Posted Date: December 28th, 2020

DOI: https://doi.org/10.21203/rs.3.rs-130307/v1

Version of Record: A version of this preprint was published at Scientific Reports on April 16th, 2021. See the published version at https://doi.org/10.1038/s41598-021-87997-z.

Abstract

In this paper, the surface enhanced Raman scattering (SERS) characteristics of Au and Au@Al_2O_3 nanoparticle dimers were calculated and analyzed by using finite element method (3D-FEM). Firstly, the electric field enhancement factors of Au nanoparticles at the dimer gap were optimized from three aspects: the incident angle of the incident light, the radius of nanoparticle and the distance of the dimer. Then, aluminum oxide is wrapped on the Au dimer. What is different from the previous simulation is that Al_2O_3 shell and Au core are regarded as a whole and the total radius of Au@Al_2O_3 dimer is controlled to remain unchanged. By comparing the distance of Au nucleus between Au and Au@Al_2O_3 dimer, it is found that the electric field enhancement factor of Au@Al_2O_3 dimer is much greater than that of Au dimer with the increase of Al_2O_3 thickness. The peak electric field of Au@Al_2O_3 dimer moves towards the middle of the resonance peak of the two materials, but the peak electric field of Au dimer is more concentrated than that of Au dimer, so that the excitation wavelength has less influence on Raman enhancement. The maximum electric field enhancement factor 583 is reached at the shell thickness of 1 nm. Our results provide a theoretical reference for the design of SERS substrate and the extension of the research scope.

Introduction

Surface-enhanced Raman scattering (SERS) technology, as a new highly sensitive spectral analysis technology, is often used to detect ultra-low concentration or even single-molecule level objects to be measured, which can provide "fingerprint" information of samples at a very high precision[1]. In recent years, due to its advantages of high sensitivity, high selectivity, little interference by water and fluorescence signal, short detection time and convenient operation, SERS technology has been widely used in material science, medicine, environmental analysis, biomolecule detection and other fields[2–4].

Since the emergence of SERS technology, various nanostructures made of noble metal nanomaterials have become a research hotspot in this filed. In the experiment, Agata *et al.* used magnetron sputtering to transfer Ag, Au and Cu nanoparticles onto TiO_2 and Ti nanotube walls to produce SERS substrate with high activity[5]. Hui He et al. [6] conducted a detailed study on the fluorescence experiments of plasma nanostructures in the core-shell of the controlled preparation of the imprinted layer mainly for the detection of plasma enhanced fluorescence for the specific heteromeric molecules. This has paved the way for the controlled preparation of the molecularly imprinted[7–10] plasma nanostructures. Kang *et al.* [11]reported a method to achieve high-speed and high resolution Raman imaging of living cells by near infrared extraction and high speed verification Raman microscopy using small spherical gold nanoparticles with high narrow nanoscale gap structure. Similarly, the application of SERS technology to molecular detection to improve the sensitivity and high speed and high spatial resolution of live cell Raman images[12–14] greatly promoted the theoretical exploration of the optimal state of metal particles under different configurations. Therefore, Tian's group of Xiamen University [15] not only calculated and analyzed the SERS and TERS configurations theoretically, but also prepared them by experimental means, which indicated the credibility of the theoretical results and broadened the scope of the research

field. At present, the methods to calculate the electric field enhancement of nanometer particle configuration mainly include 3D finite difference time domain (3D-FDTD) and 3D-FEM. Anitharaj *et al.*[16] used the FDTD method to study the local electric field of Ag@SiO_2 trimer. By gradually breaking the symmetry of the trimer nanospheres, the dependence of two kinds of orthogonal polarization on the plasma wavelength was analyzed. However, the FEM is more trial for small scale nanostructures, and the appropriate excitation wavelength energy is selected to maximize the sensitivity of SERS configuration.

In this paper, 3D-FEM was used to calculate the influence of the wavelength, the angle of incident light, the dimer distance and the radius of the nanoparticle on the electric field enhancement factor. It is found that the electric field enhancement distance is dominant for the dimer gap. After the optimal size model was obtained, Al_2O_3 was coated on the surface of Au dimer, and the influence of Al_2O_3 thickness on electric field enhancement and Raman enhancement factor were calculated. The results show that the ratio of The Raman enhancement factor of Au@Al_2O_3 dimer to that of Au dimer increases with the increase of the thickness of Al_2O_3 shell. The calculated results not only reasonably explain the SERS enhanced mechanism of Al_2O_3 as the shell material, but also expand the research scope of SERS technology, which have certain guiding significance for the SERS substrate of high sensitivity Al_2O_3 shell.

Theoretical Model And Calculation Method

Figure 1 demonstrate our theoretical model. The single Au nanosphere, Au dimer and Au@Al_2O_3 were calculated by placing the electric dipole in the same position. It is clearly seen from the Fig. 1 that with the further study of configuration, the enhancement factor is constantly increasing. The model of Au@Al_2O_3 dimer is composed of two metal spheres, in which the radius of the metal sphere is r, the thickness of the shell is r_0 and the distance between dimers is d. During the modeling process, the wavelength of the plane wave incident to the system is set as λ, the angle of the incident light is set as θ, and the electric field E in the polarization direction is perpendicular to the line between the two centers of the dimer. In the simulation, $E0(\lambda)$ of the incident electric field is set as 1V/m for ease of calculation. In order to prevent the impact of the reflection field at the boundary on the calculation results, a perfectly matched layer (PML) is used to cover the whole simulation area. Meanwhile, to ensure the accuracy and reliability of simulation data, the degree of freedom in the program reached more than 2.5 million. Finally, an oscillating point electric dipole is used to represent the molecular radiation in the middle of the metal sphere, and various physical parameters of Au and Au@Al_2O_3 dimer are calculated and analyzed theoretically. The local surface plasmon resonance (LSPR) generated by Au dimer can greatly enhance the Raman signal strength of the target molecule to be measured. Raman enhancement factor is mainly related to two local electric field enhancement factors: the excitation field enhancement factor $|M(\lambda I)|=|E(\lambda I)|/|E0(\lambda I)|$ and the emission field enhancement factor $|M(\lambda s)|=|E(\lambda s)|/|E0(\lambda s)|$ are generated by the interaction of the incident and emitted light fields with the equidistant exciter on the surface of Au. Here, λI and λs represent the wavelength of the incident laser and scattered laser respectively. $E0(\lambda)$ and $E(\lambda)$ represent the intensity of incident and locally enhanced electric fields of the molecules. Finally, the formula for calculating the Raman enhancement factor is[17,18]:

$RE = |M(\lambda l)|^2 |M(\lambda s)|^2 = (|E(\lambda l)|/|E0(\lambda s)|)^2 (E(\lambda s)|/|E0(\lambda l)|)^2$ (1)

Where $E(\lambda l)$ is the local electric field intensity, and $E(\lambda s)$ is the field intensity of the radiation light field with the radiation wavelength λs. The radius of $Au@Al_2O_3$ dimer is calculated as follows: $R = r + r_0$. Where R is the radius of $Au@Al_2O_3$ dimer, r is the radius of the Au nucleus, and r_0 is the thickness of Al_2O_3 layer. The distance between the dimers is air, and d represents the distance between the dimers. Then, the SERS performance of Au dimers and $Au@Al_2O_3$ dimers was compared by wrapping Al_2O_3 outside Au nucleus. The distance between Au nanospheres of $Au@Al_2O_3$ dimer is defined as: $D = r_0 + d$. Where, D is the distance between $Au@Al_2O_3$ dimer Au nanospheres, R_0 is the thickness of Al_2O_3 layer, and d is the distance between $Au@Al_2O_3$ dimer.

As can be seen from the right side of Fig. 1, compared with a single Au nanospheres, the nanoscale cavity formed between Au dimers makes the electric field more localized, thus forming a highly localized nanoscale spatial resolution. Then $Au@Al_2O_3$ dimer because of Al_2O_3 shell indirectly shorten the distance between the dimers, so that the spatial resolution is improved again. With the continuous optimization of the structure, the simulation results show that the electric field enhancement factor and spatial resolution are further improved.

Results And Discussion

In the simulation, the influence of incident light angle on the enhancement factors of electric field and Raman scattering is discussed in Fig. 2. The radius of Au nanospheres is set as 50 nm, and the distance between the two Au nanopheres is set to 2 nm. Selected light source is linearly polarized plane wave, and the measurement was made every 15° from the X-axis to the Z-axis, so as to discuss its influence on the enhancement performance of the system, as shown in Fig. 2. Figure 2 (a) shows that the electric field enhancement factor decreases gradually when the incident angle increases from 0 ° ~ 90 °. It is noticed that, the wavelength of the peak position is kept 635 nm and does not change with the angle. This may be because the light absorption property of the material is independent of the change of the incident angle, but related to the configuration of Au dimer. Figure 2 (b) shows the field distribution of Au dimer with the radius of 50 nm and distance of 2 nm under the excited wavelength of 635 nm. Hot spots on the electric field have been greatly enhanced and localized area to the nanometer gap, which is due to the surface from excimer phenomenon, such as that in the resonance state of electromagnetic field energy is efficiently into the metal surface free electrons collective vibrational energy. The red area represents a relative stronger electric field, which demonstrate that the electromagnetic field is enhanced and limited within the scope of the metal surface. Moreover, it can be seen that the electric field strength of dimer gap at $\theta = 0°$ is significantly higher than that at $\theta = 60°$ on the same scale,which is because vertical incidence maximizes the vertical field component[19].

In order to optimize the local electric field and the Raman enhancement, the radius of Au nanospheres should be considered, as shown in Fig. 3. By fixing the angle of incidence $\theta = 0°$ and the distance between nanoparticles $d = 2$ nm, the radius of Au dimer is calculated in the range from 10 nm to 70 nm. It can be

clearly seen in Fig. 3(a) that the electric field enhancement factor is very small when r = 10 nm, and there are the obvious resonance peaks for the electric field enhancement between 20 nm and 70 nm. With the increase of the radius, the peak value of the electric field enhancement factor gradually increases and then decreases. When r = 50 nm and λI = 635 nm, the electric field enhancement reaches the maximum value of around 220, and then the peak begins to decline. It is noticed that the width of the wave peak increases, which make the excitation wavelength broaden when calculating the Raman enhancement factor, and thus the application of Au dimer becomes wider. With the increase of the radius, it is found that the peak value of the electric field enhancement factor is red shifted obviously, and the corresponding resonance wavelength is shifted from 545 nm to 740 nm. The red shift of the peak is mainly due to the Au nuclear on both sides of the opposite sign of surface charge between the restoring force of abate[20]. For the larger Au nuclear radius, the distance between the surface charge increase results in the decrease of the interaction of the dimer. Therefore, the restoring force between them will be abated, resulting in a red shift phenomenon of the LSPR peak. Figure 3(a) shows that the electric field enhancement factor is the largest with the excited wavelength of 635 nm, which is used as the excitation wavelength to calculate the Raman enhancement factor with different radius according to formula (1), as shown in Fig. 3(b). When r = 50 nm, the Raman enhancement factor achieve 10^9 at around 535 nm ~ 675 nm, and the maximum Raman enhancement factor is 2.4×10^9 at 635 nm, which will continue to increase with subsequent structural optimization. In the simulation process, it is assumed that the incident wavelength is 635 nm, that is, the Stokes scattering wavelength in Raman scattering should be greater than 635 nm. Therefore, r = 60 nm Raman enhancement factor is larger in the range from 635 nm to 735 nm, and thus the stronger molecular SERS signals can be obtained. However, it is worth noting that when r = 40 nm, due to its maximum enhancement factor around 600 nm, it is conducive to the measurement of An-Stokes scattered waves[21]. The Au dimer at this excitation wavelength is very conducive to the non-destructive detection of living cells in life sciences[22,23].

In order to find the configuration of Au dimer with better enhancement effect, the influence of the distance between Au dimers on the electric field and the Raman enhancement factor is studied by fixing the Au radius of 50 nm and the angle of incident angle of 0°, and the simulation results are shown in Fig. 4. With the decrease of the distance between dimers, the peak value of the electric field enhancement factor appears obvious red shift, and it gradually increases with the decrease of the distance from 3 nm to 1 nm. However, when the distance continues to be reduced to 1 nm, the enhancement factor has a multiple enhancement compared with other distance in the whole simulation range, and reaches the maximum value of around 583 under the excited wavelength of 675 nm. The peak value of enhancement factor is 1.5 ~ 3 times for the other peaks. The intensity of the electric field decreases slightly at 600 nm ~ 650 nm and then peaks, probably due to the interference of incident light with the scattered radiation[24]. This electric field enhancement factor is a very groundbreaking discovery and provided a reliable data support for SERS development. Figure 4(b) also calculates the Au dimer Raman enhancement factor at excitation wavelength of 635 nm. At d = 3 nm, the Raman enhancement factor is generally lower than other distance enhancement factors, but the peak value of the Raman enhancement factor is also up to 10^8, which can meet general experimental requirements of molecule characterization and recognition.

The peak value of Raman enhancement factor is above 10^9 when the gap distance is the range from 1 nm to 2 nm, especially for d = 1 nm, the maxiumum value of Raman enhancement factor reaches 7.8×10^{10}, which is far beyond the experimental requirements of single molecule characterization and recognition imaging.

For the spherical dimer structure, the influence of radius change on the position of the electric field peak is greater than that of the distance. For Au@Al_2O_3 core-shell structure, the total control radius is R = 50 nm. Figure 5 (a) (b) shows the curve of electric field enhancement factor and Raman enhancement factor with the change of incident light wavelength in the case of Au@Al_2O_3 dimer with spacing d = 1 nm and total radius R = 50 nm. With the increase of the thickness of Al_2O_3, the peak value of the electric field enhancement factor gradually decreases and shows a blue shift, which has certain guiding significance to the selection of SERS substrate material and the selection of excitation wavelength. Under the condition of constant radius, Fig. 5 (c) clearly shows from the side diagram and top view of the electric field distribution that the electric field will gradually decrease with the gradual increase of the thickness of Al_2O_3. This is mainly because the thickness of the shell increases the distance between Au nuclei[25]. Depending on Su's[26] paper, the resonance spectrum of Al is in the near ultraviolet spectrum, while that of Au is in the visible spectrum. Therefore, it is speculated that the Al_2O_3 covering the surface of the Au nucleus leads to the blue shift of the electric field enhancement factor. Compared with the Au dimer in Fig. 4 (a), the peak value of the electric field enhancement factor in Au@Al_2O_3 dimer is relatively concentrated. This led us to speculate whether the core-shell structure of two different materials would cause the resonance peak to move towards the resonance peak of the other material, eventually leading to a concentration of formant positions.

Figure 6 shows the comparison of Raman enhancement factors at different distances of Au and Au@Al_2O_3 dimers corresponding to different excitation wavelengths. At Au dimers r = 50 nm, the spectral position corresponding to the maximum electric field enhancement factor with distance from 1 nm to 3 nm is selected as the excitation spectrum, i.e. λex = 620 nm, 625 nm, 635 nm, 650 nm, 675 nm and the Raman enhancement factor with distance d = 2 nm, 3 nm is calculated. Figure 6 (b) and (d) respectively represent the spectral position corresponding to the maximum electric field enhancement factor of Au@Al_2O_3 at R = 50 nm, dimer distance d = 1 nm, shell thickness r_0 = 1 nm ~ 4 nm as the excitation spectrum. At λex = 635 nm,640 nm,650 nm,665 nm, the Raman enhancement factors of Au@Al_2O_3 dimer at D = 2 nm and 3 nm are calculated. It can be seen from Fig. 6 (a) and (b) that the strength of Au@Al_2O_3 dimer is greater than that of Au dimer at the same distance. With the comparison of Fig. 6 (c) and (d), it is found that with the increase of Al_2O_3 thickness, the increase times of electric field enhancement factor will gradually increase. Therefore, it is quite meaningful to wrap Al_2O_3 material on the Au core shell. At the same distance, there is a certain difference in the Raman enhancement factor under different excitation wavelengths, but it is basically in an order of magnitude, which also shows that the Au dimer has a wider excitation spectrum under different distance, making its application scope wider[27]. Figure 6 shows that the influence of excitation wavelength on the final Raman enhancement factor of the final model with the

increase of the thickness of Al_2O_3, however the influence of excitation wavelength on the final Raman enhancement factor of Au dimer increases with the increase of distance. The reason may be that Al_2O_3 as shell material makes Au@Al_2O_3. The resonance absorption peak of dimer is more concentrated, which leads to Au@Al_2O_3 When spherical dimer is used as SERS substrate configuration, it is easier to select excitation wavelength. It can be found from the Fig. 6 that slight changes in each configuration will change the corresponding optimal excitation wavelength, so the theoretical simulation is very meaningful. The results show that the Raman enhancement of Au@Al_2O_3 dimer is very sensitive to distance, and the wrapped Al_2O_3 can transfer the Raman enhancement of Au core well. Currently, the materials used for SERS substrate are generally precious metals, and the preparation cost is relatively high, thus resulting in the appearance of the shell structure. With the progress of subsequent manufacturing methods, ultra-high sensitivity SERS signals were provided for living cell detection and biological imaging[28], and further understanding of cell changes is promoted.

Conclusion

In this paper, the effects of electric field enhancement and Raman enhancement of the molecular system in the middle of Au and Au@Al_2O_3 dimer are studied by using 3D-FEM. The results show that the enhancement of SERS depends on the angle and wavelength of incident light, the radius of Au nanoparticles and the distance between dimers, but the distance between dimers dominates. When $\theta = 0°$, $r = 50$ nm and $d = 1$ nm, the local surface plasmon resonance coupling in the Au dimer nanometer gap produces a maximum electric field enhancement factor of 583, and reaches the maximum Raman enhancement factor of 1.5510^{11} at the excitation wavelength of 675 nm. By wrapping Al_2O_3, the distance between Au dimer is indirectly shortened, which leads to the enhancement of the electric field factor. The results demonstrate that the ratio of the Raman enhancement factor of Au@Al_2O_3 dimer to that of Au dimer increases with the increase of the thickness of Al_2O_3 shell. This is mainly because the refractive index of Al_2O_3 is greater than that of air. Under the condition that Au core is at the same distance, the thickness of Al_2O_3 also determines the thickness of the larger refractive index region. Au@Al_2O_3 dimer Raman enhancement factor also up to 10^9, satisfying the experimental requirements of single molecule detection. Al_2O_3 has added to Au nucleus to adjust the maximum spectral peak position of LSPR coupling and make the peak position become centralized. Not only widened the scope of SERS research, but also broadened the application scope of SERS detection technology. The theoretical results have good guiding significance for studying the internal mechanism of various SERS detection with high sensitivity[29,30].

Declarations

Acknowledgment

This work was supported by the Natural Science Foundation of Hebei province (No. B2018203112).

Author Contributions

B.-X.Y., W. Y.and Y.-Y. Z. proposed the idea. B.-X.Y. performed the simulations. All authors were involved in discussion and analysis of the manuscript. The manuscript was written by B.-X.Y., W. Y. and Y.-Y. Z.

Competing Interests

The authors declare that they have no competing interests.

References

1. Huang, Q. *et al.* Synthesis of uniform Ag nanosponges and its SERS application. *Spectrochimica Acta Part A: Molecular and Biomolecular Spectroscopy* **201**, 300–305, DOI: https://doi.org/10.1016/j.saa.2018.05.019 (2018).
2. Kleinman, S. L., Frontiera, R. R., Henry, A. I., Dieringer, J. A. & Van Duyne, R. P. Creating, characterizing, and controlling chemistry with SERS hot spots. *Physical Chemistry Chemical Physics* **15**, 21–36, DOI: https://doi.org/10.1039/c2cp42598j (2013).
3. Zhang, Z., Yang, P., Xu, H. & Zheng, H. Surface enhanced fluorescence and Raman scattering by gold nanoparticle dimers and trimers. *Journal of Applied Physics* **113**, 033102, DOI: https://doi.org/10.1063/1.4776227 (2013).
4. Zhang, X. *et al.* Recent progress in the fabrication of SERS substrates based on the arrays of polystyrene nanospheres. *Science China-physics Mechanics & Astronomy* **59**, 126801, DOI: https://doi.org/10.1007/s11433-016-0341-y (2016).
5. Roguska, A., Kudelski, A., Pisarek, M., Opara, M. & Janikczachor, M. Surface-enhanced Raman scattering (SERS) activity of Ag, Au and Cu nanoclusters on TiO2-nanotubes/Ti substrate. *Applied Surface Science* **257**, 8182–8189, DOI: https://doi.org/10.1016/j.apsusc.2010.12.048 (2011).
6. He, H. *et al.* Controllably prepared molecularly imprinted core-shell plasmonic nanostructure for plasmon-enhanced fluorescence assay. *Biosensors and Bioelectronics* **146**, 111733,DOI: https://doi.org/10.1016/j.bios.2019.111733 (2019).
7. Jiang, C., Wu, T., Liu, J. & Wang, Y. Application of a thermo-sensitive imprinted SERS substrate to the rapid trace detection of ofloxacin. *Analytical methods: advancing methods and applications* **12**, 4783–4788, DOI: https://doi.org/10.1039/D0AY00616E (2020).
8. Li, H. J. *et al.* Multifunction Sandwich Composite SERS Imprinted Sensor Based on ZnO/GO/Ag for Selective Detection of Cyfluthrin in River. *ChemistrySelect* **5**, 6475–6481, DOI: https://doi.org/10.1002/slct.202001155 (2020).
9. Xu, Y., Hassan, M. M., Ali, S., Li, H. H. & Chen, Q. S. SERS-based rapid detection of 2,4-dichlorophenoxyacetic acid in food matrices using molecularly imprinted magnetic polymers. *Microchim. Acta* **187**, 9, DOI: https://doi.org/10.1007/s00604-020-04408-2 (2020).
10. Yang, Y.-Y. *et al.* Controllable in situ fabrication of portable AuNP/mussel-inspired polydopamine molecularly imprinted SERS substrate for selective enrichment and recognition of phthalate

plasticizers. *Chemical Engineering Journal* **402**125179, DOI: https://doi.org/10.1016/j.cej.2020.125179 (2020).

11. Kang, J. W., So, P. T. C., Dasari, R. R. & Lim, D. High Resolution Live Cell Raman Imaging Using Subcellular Organelle-Targeting SERS-Sensitive Gold Nanoparticles with Highly Narrow Intra-Nanogap. *Nano Letters* **15**, 1766–1772, DOI: https://doi.org/10.1021/nl504444w (2015).
12. Zhang, Y., Jimenez de Aberasturi, D., Henriksen-Lacey, M., Langer, J. & Liz-Marzan, L. M. Live-Cell Surface-Enhanced Raman Spectroscopy Imaging of Intracellular pH: From Two Dimensions to Three Dimensions. *ACS sensors* **5**, 3194–32060c01487, DOI: https://doi.org/10.1021/acssensors.0c01487 (2020).
13. Gu, Y., Bi, X. & Ye, J. Gap-enhanced resonance Raman tags for live-cell imaging. *Journal Of Materials Chemistry B* **8**, 6944–6955, DOI: https://doi.org/10.1039/d0tb00659a (2020).
14. Koike, K. *et al.* Alkyne-tag SERS imaging for visualizing small molecule drugs in live cells, Spie-Int Soc Optical Engineering, Bellingham, DOI: https://doi.org/10.1117/12.2545872 (2020).
15. Ding, S.-Y., You, E.-M., Tian, Z.-Q. & Moskovits, M. Electromagnetic theories of surface-enhanced Raman spectroscopy. *Chemical Society Reviews* **46**, 4042–4076, DOI: https://doi.org/10.1039/c7cs00238f (2017).
16. Nagarajan, A., Panchanathan, A. P., Chelliah, P., Satoh, H. & Inokawa, H. Optimization of electric field enhancement of Ag@SiO2 trimer nanospheres by finite difference time domain method. *Applied Surface Science* **495**, 143547, DOI: https://doi.org/10.1016/j.apsusc.2019.143547 (2019).
17. Yamamoto, Y. S. & Itoh, T. Why and how do the shapes of surface-enhanced Raman scattering spectra change? Recent progress from mechanistic studies. *Journal of Raman Spectroscopy* **47**, 78–88, DOI: https://doi.org/10.1002/jrs.4874 (2016).
18. Johansson, P., Xu, H. & Käll, M. Surface-enhanced Raman scattering and fluorescence near metal nanoparticles. *Physical Review B* **72**, 035427, DOI: https://doi.org/10.1103/physrevb.72.035427 (2005).
19. Yang, Z., Aizpurua, J. & Xu, H. Electromagnetic field enhancement in TERS configurations. *Journal of Raman Spectroscopy* **40**, 1343–1348, DOI: https://doi.org/10.1002/jrs.2429 (2009).
20. Kudelski, A. & Bukowska, J. Charge-transfer contribution to surface-enhanced Raman scattering and surface-enhanced resonance Raman scattering of dyes at silver and gold electrodes. *Chemical Physics Letters* **253**, 246–250, https://doi.org/10.1016/0009-2614(96)00252-7 (1996).
21. Koo, T. W., Gerth, C. M. & Yamakawa, M. Method and device for detecting a small number of molecules using surface-enhanced coherant anti-stokes raman spectroscopy. DOI: https://doi.org/US20050084980 A1 (2005).
22. Franco, D., Plano, L. M. D., Rizzo, M. G., Scibilia, S. & Mezzasalma, A. M. Bio-hybrid gold nanoparticles as SERS probe for rapid bacteria cell identification. *Spectrochimica Acta Part A Molecular and Biomolecular Spectroscopy* **224**, 117394, https://doi.org/10.1016/j.saa.2019.117394 (2019).
23. Li, L., Si, Y., He, B. & Li, J. Au-Ag alloy/porous-SiO 2 core/shell nanoparticle-based surface-enhanced Raman scattering nanoprobe for ratiometric imaging analysis of nitric oxide in living cells. *Talanta*

205, https://doi.org/10.1016/j.talanta.2019.120116 (2019).

24. Mohammadnezhad, M., Saeed, S. R. & Hassanzadeh, A. Theoretical simulation of Gaussian beam interferometric optical tweezers with symmetrical construction. *Journal of optics* **21**, DOI: https://doi.org/10.1088/2040-8986/ab406b (2019).
25. Wei, Y., Li, L., Sun, D. X., Zhu, Y. Y. & Tian, G. J. The effect of silica shell on the surface enhanced Raman scattering and fluorescence with Ag nanoparticles: A three-dimensional finite element method investigation. *Optics Communications* **427**, 426–432, DOI: https://doi.org/10.1016/j.optcom.2018.06.086 (2018).
26. Su, D. *et al.* Facile fabrication of configuration controllable self-assembled Al nanostructures as UV SERS substrates. *Nanoscale* **10**, 22737–22744, DOI: https://doi.org/10.1039/c8nr08555b (2018).
27. Trotsiuk, L. *et al.* Plasmon-enhanced fluorescence in gold nanorod-quantum dot coupled systems. *Nanotechnology* **31**, 105201, DOI: https://doi.org/10.1088/1361-6528/ab5a0e (2020).
28. Capocefalo, A. *et al.* Exploring the Potentiality of a SERS-Active pH Nano-Biosensor. *Frontiers in chemistry* **7**, DOI: https://doi.org/10.3389/fchem.2019.00413 (2019).
29. Wu, H., Chen, T., Tsai, H. & Chen, C. Au Nanoparticles Deposited on Magnetic Carbon Nanofibers as the Ultrahigh Sensitive Substrate for Surface-Enhanced Raman Scattering: Detections of Rhodamine 6G and Aromatic Amino Acids. *Langmuir* **34**, 14158–14168, DOI: https://doi.org/10.1021/acs.langmuir.8b02488 (2018).
30. Liu *et al.* Liquid-liquid interfacial self-assembled Au NP arrays for the rapid and sensitive detection of butyl benzyl phthalate (BBP) by surface-enhanced Raman spectroscopy. *Analytical & Bioanalytical Chemistry*, DOI: https://doi.org/10.1007/s00216-018-1184-6 (2018).

Figures

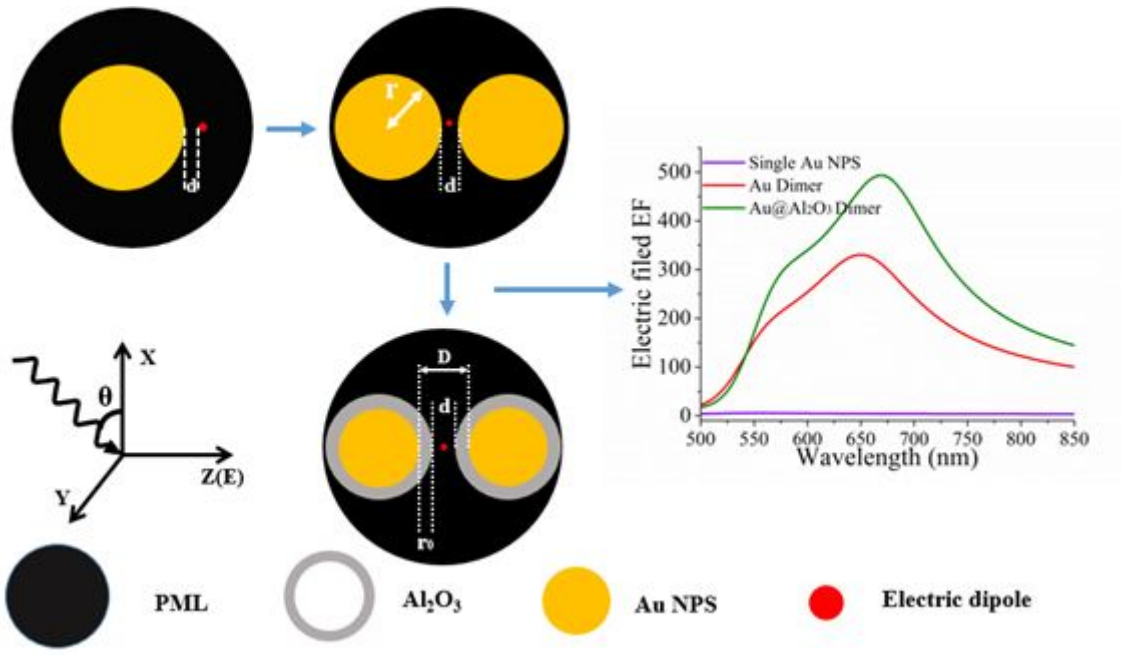

Figure 1

theoretical model of Au and Au@Al2O3 dimer. On the right is the comparison diagram of the electric field enhancement factors of Au and Au@Al2O3 dimer and a single sphere.

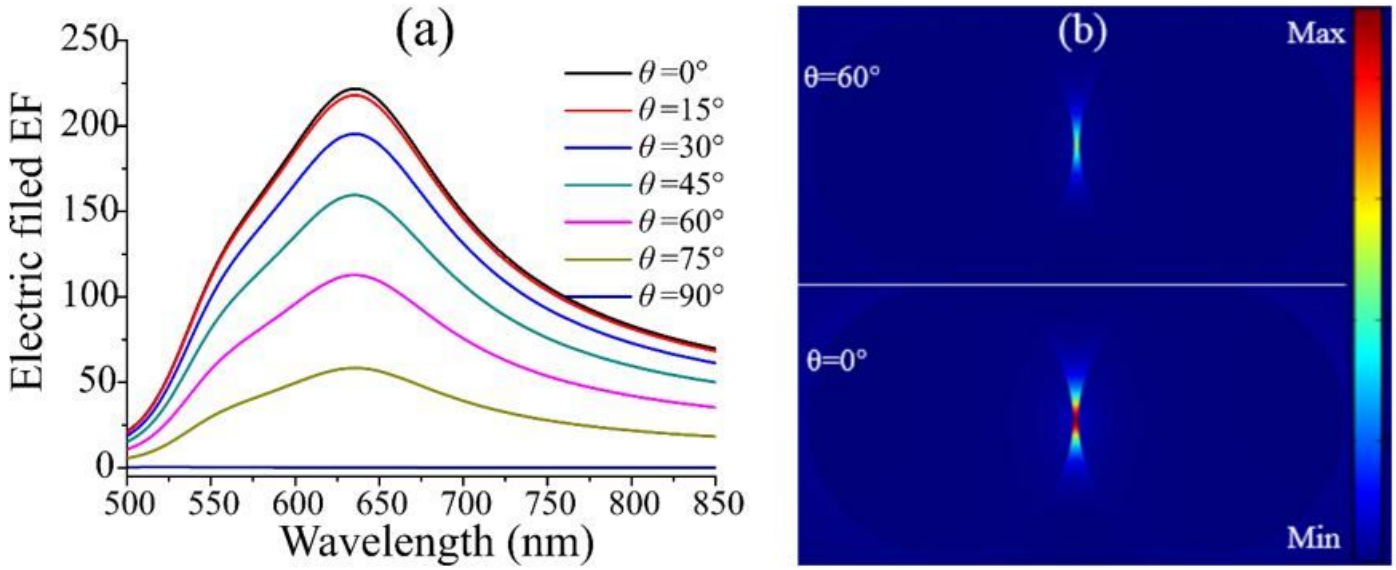

Figure 2

(a) The influence of the angle of incident light on the surface enhanced local electric field of Au dimer. Here we set d=2 nm, r=50 nm. (b) The electric field distribution at θ=60° and θ=0° with the excitation wavelength of 635nm. The two electric field distributions are drawn on the same scale.

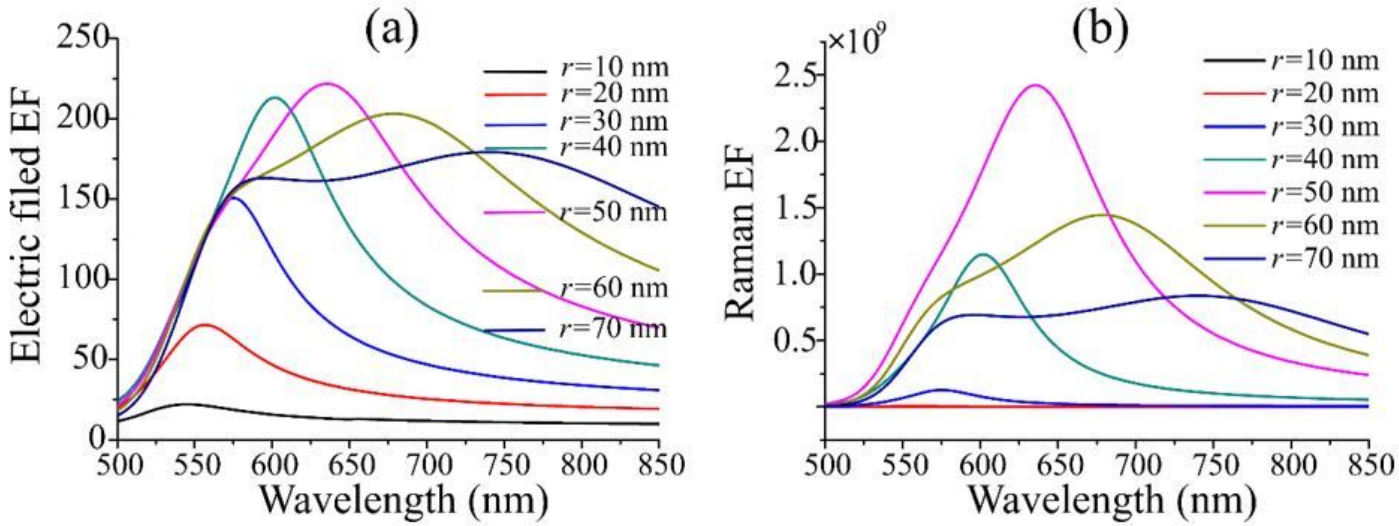

Figure 3

The dependence of the electric field enhancement factor (a) and Raman enhancement factor (b) of Au dimer on with the variation of incident light wavelength at different radius. Here the incident angle is set

as 0°, the distance of Au nanoparticles is 2 nm, and the excitation wavelength is set as 635 nm.

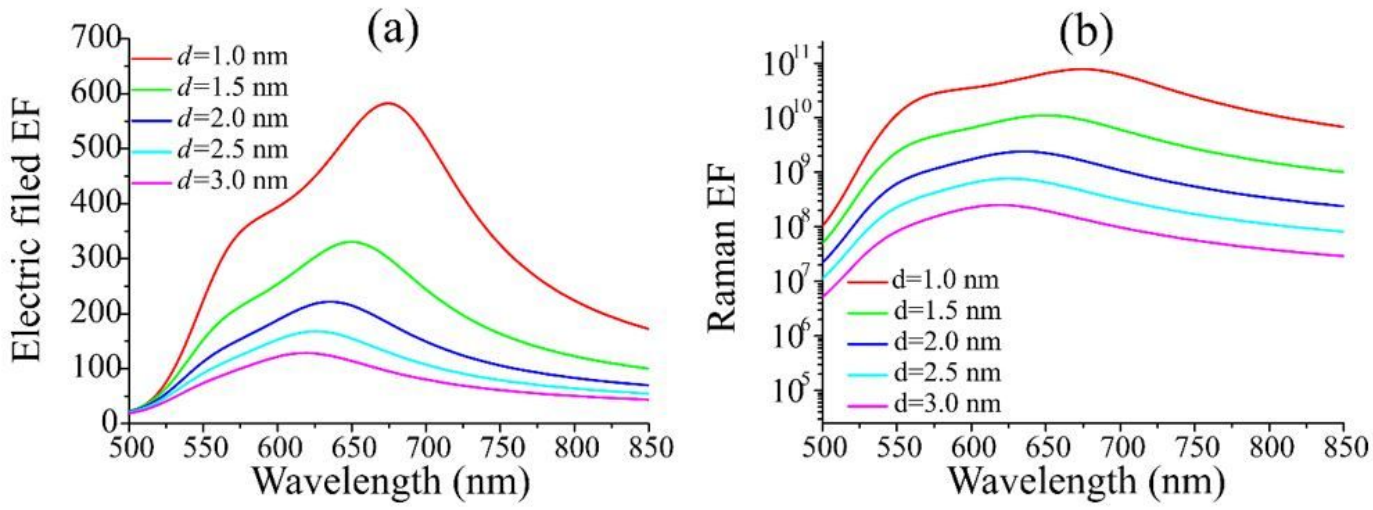

Figure 4

The relation curves of electric field intensity enhancement factor (a) and Raman enhancement factor (b) with the variation of incident light wavelength at different distance between Au dimers. The incident angle is 0°, the radius of Au nanospheric particle is 50 nm, and the excitation wavelength of Raman enhancement factor is 635 nm.

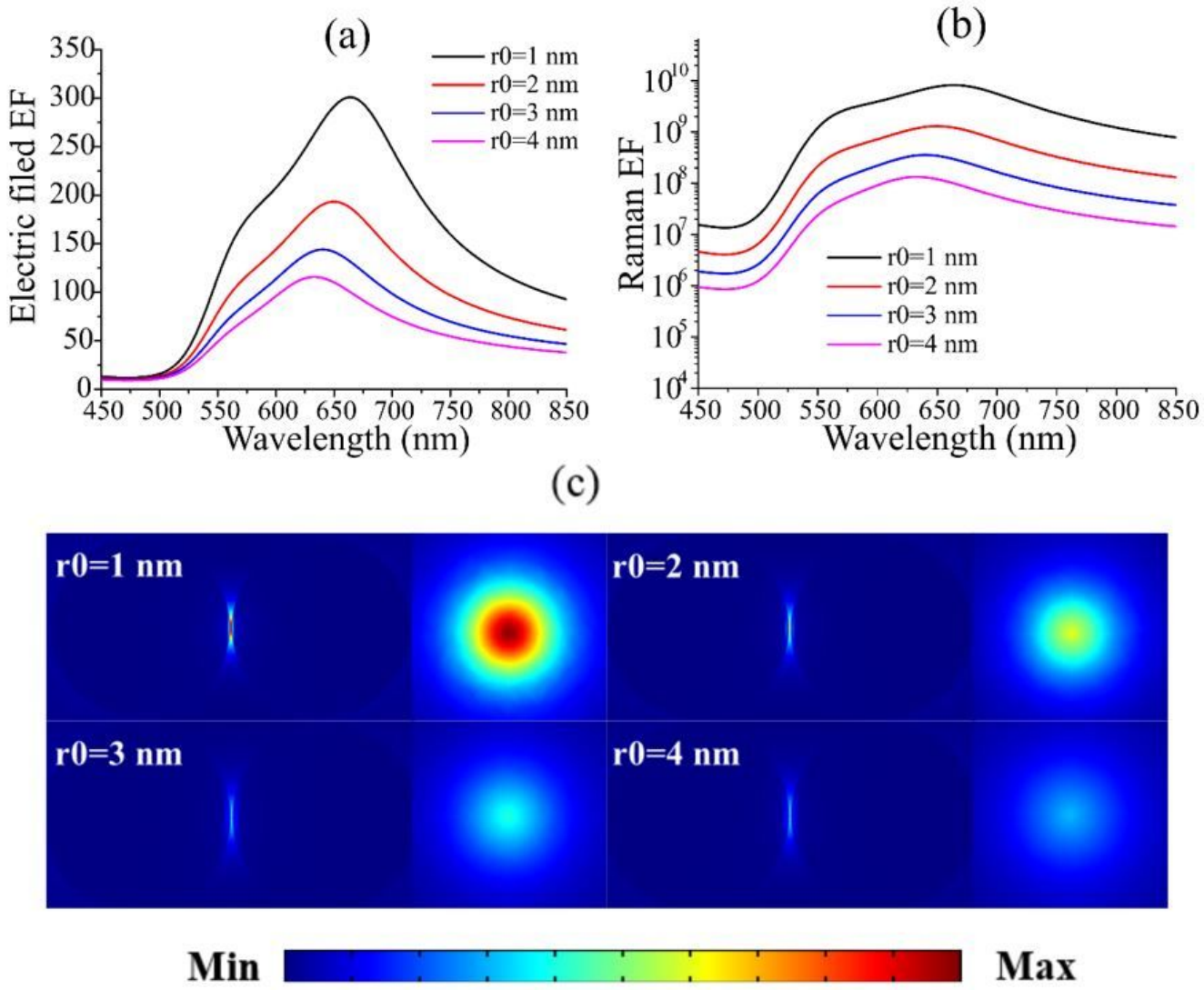

Figure 5

The relation curve of electric field enhancement (a) and Raman enhancement factor (b) covering different Al2O3 thickness with the change of incident light wave- length. (c) Is the side view and top view of electric field distribution with different thickness Al2O3(r0 =1-6 nm). The excitation wavelength of the Raman enhancement factor and the electric field distribution diagram are both 665 nm. The distance between Au@Al2O3 dimer is fixed at 1nm, and the radius R is set to 50 nm.

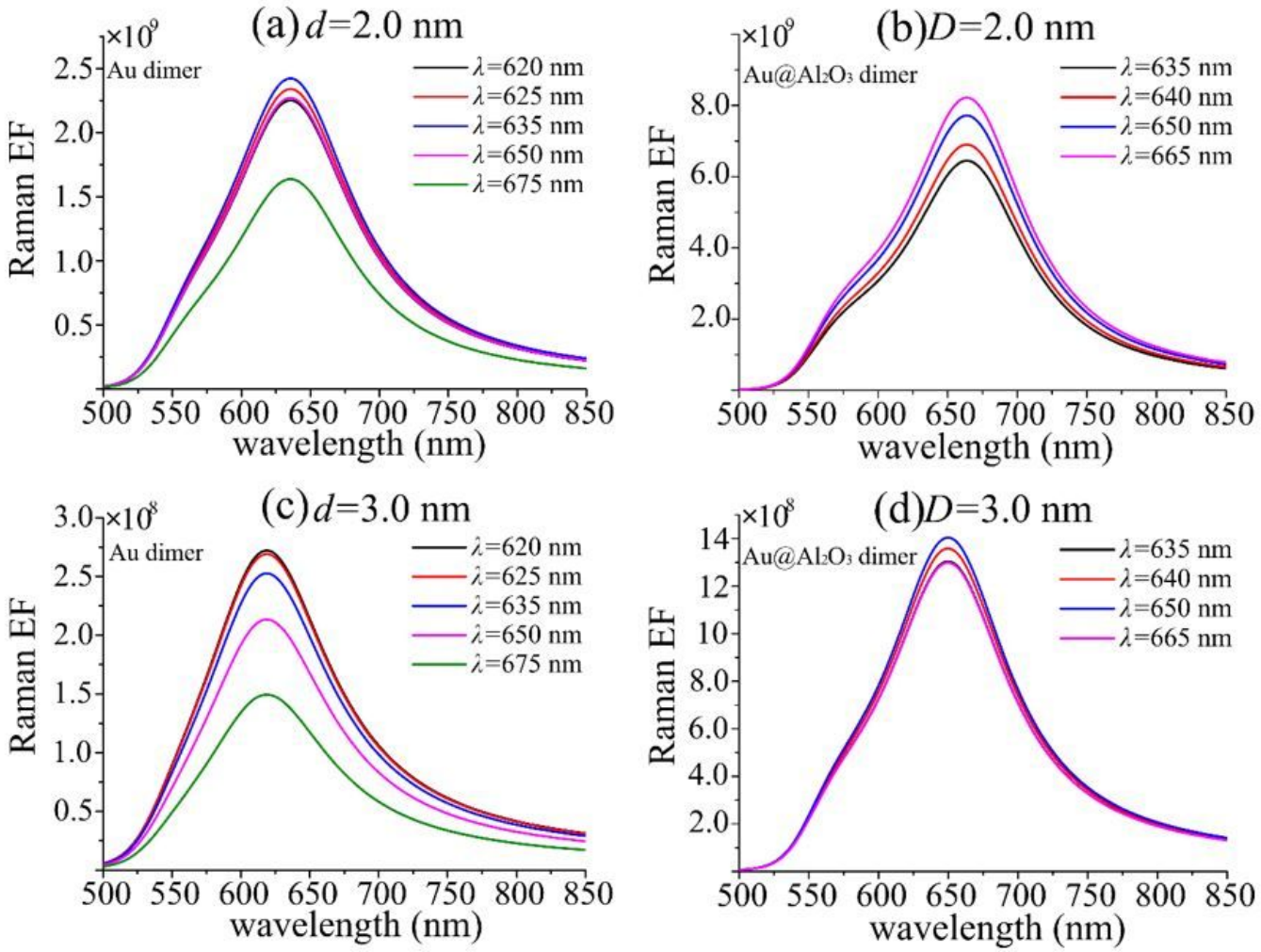

Figure 6

(a) (c) and (b) (d) respectively represent the comparison of Raman enhancement factor curves of Au and Au@Al2O3 dimers with different excitation wavelengths at different distances, with a radius of 50 nm and incident light angle of 0°. The distance between Au@Al2O3 dimer is set as d=1 nm, and the thickness of Al2O3 shell is r0=1 nm and 2 nm respectively, so the distance between Au@Al2O3 dimer Au core is D=2 nm and 3 nm.